Journal of Computers Vol. 35 No. 5, October 2024, pp. 169-186
doi: 10.53106/199115992024103505012

Trajectory Planning Method for Welding Pipe Parts Using Industrial Robots Based on 3D Vision

Rui Fan[1,2,3*], Jian Gao[1,3], Chun-Ying Zhu[1,4], and Qing-Chuan Liu[1,2,3]

[1] Hebei Institute of Mechanical and Electrical Technology,
Xingtai City 054000, Hebei Province, China
{fanrui98792, jian797, yingying999, qingchuan3978}@126.com

[2] Hebei Province Electromechanical Equipment Intelligent Perception and Advanced Control Technology Innovation Center, Xingtai City 054000, Hebei Province, China

[3] Xingtai Intelligent Production Line and Equipment Technology Innovation Center,
Xingtai City 054000, Hebei Province, China

[4] Xingtai Intelligent Factory Monitoring and Network Technology Innovation Center,
Xingtai City 054000, Hebei Province, China

Received 26 September 2024; Revised 2 October 2024; Accepted 17 October 2024

Abstract. Pipe parts are generally made of circular tubes, and intersecting lines are formed at the junction of two circular tube parts. This article uses 3D vision to identify the weld seam and then guides the welding robot to complete the welding. Firstly, a welding system including welding robots, robot control cabinets, welding machines, surface structured light vision sensors, industrial computers, teaching devices, etc. was built according to production needs. Based on the system configuration, the hand eye calibration of the Eye- to -Hand vision system structure was completed. Then, for the extraction of pipe welds, the first step is to complete the extraction of weld seam features. The second step is to denoise the noise in the feature image. The third step is to fit the denoised image into a three-dimensional welding trajectory. Optimal, based on the fitted welding trajectory, the planning of the weld seam path and the optimization of the industrial robot welding path were completed. Welding simulation experiments were designed and completed for the intersecting line trajectory of pipe welding, verifying the effectiveness of the method proposed in this paper.

Keywords: 3D vision, industrial robot, steel pipe, planning, feature extraction

1 Introduction

In recent years, with the rapid development of technology, industrial robot technology has gradually become a highly concerned field. Industrial robots are gradually replacing workers in industrial production to complete automated production work, and can achieve efficient and stable continuous production. Among them, welding processing is one of the common work areas of industrial robots, such as automobile body welding, large ship welding processing, etc. For the traditional welding processing industry, limited by the characteristics of small product audience, limited product quantity, and diverse product types, there is still a reliance on manual welding to complete production work, and it has not been well integrated with industrial robots and automated welding processing technology. Welding processing belongs to high-strength and high-risk occupations, and welding workers cannot achieve uninterrupted production operations around the clock. At the same time, due to the different welding levels of welding workers with different qualifications, it is impossible to ensure the consistency of product quality. Therefore, traditional manual welding processing products generally have the production characteristics of low processing efficiency and high overall repair rate. Therefore, using industrial robots to achieve automatic welding in traditional parts welding and processing can effectively improve the accuracy and processing efficiency of traditional welding, improve the working environment of workers, and ensure the quality of welded products [1].

The welding industrial robots currently used in practical production applications can be divided into three categories in terms of usage: teaching and reproduction type, offline programming type, and autonomous welding type robots. Teaching demonstration and offline programming can be classified as conventional welding robot

* Corresponding Author

usage methods. The robot implements continuous welding operations according to the path program and generated welding trajectory taught by the operator. In actual operation, there are many complex situations. When errors occur in the machining size of the workpiece or during installation, robots with strict requirements for welding conditions can only perform welding operations on the target according to the path and corresponding parameters designed by the program, and cannot make corresponding adjustments according to various situations that may occur at any time. Moreover, the accuracy of teaching and offline programming methods mostly depends on the technical level of the operator. When the complexity of welding targets and personalized customization work increase, it can lead to situations where robots cannot guarantee the quality and efficiency of welding operations during the welding process, making it difficult for robot welding technology to be deeply applied in various fields [2].

Autonomous welding robots use recognition devices such as machine vision and laser sensors to obtain weld seam related information, and based on the information obtained by sensors, achieve welding position recognition and autonomous guidance of welding trajectories, effectively improving the work efficiency and automation level of robot welding. Visual sensors are widely used in intelligent welding due to their non-contact characteristics, rich information, high accuracy, fast detection speed, and strong adaptability. Among visual sensors, active visual sensors based on structured light have the advantages of high accuracy, fast measurement speed, and good anti-interference performance. In the field of welding, structured light visual sensors are a key perception tool that can obtain three-dimensional information of the workpiece, thereby achieving accurate recognition of the position of the weld seam trajectory. This article also uses structured light cameras to complete the work done in this article [3].

Regarding the welding of pipe components, this article mainly studies the welding trajectory of the intersecting line of travel during the docking process of two pipe components. Therefore, the work done in this article is as follows:

1) Firstly, a welding system was built according to production needs, including welding robots, robot control cabinets, welding machines, surface structured light vision sensors, industrial computers, teaching devices, etc;

2) Completed the hand eye calibration of the Eye-to-Hand visual system structure, Improved recognition accuracy;

3) For the extraction of pipe welds, the weld seam features are first extracted, and then the noise in the feature image is denoised. The denoised image is then fitted into a three-dimensional welding trajectory.

4) Based on the fitted trajectory, the path following and optimization of the weld seam were completed, and the welding simulation of the intersecting line trajectory was completed, verifying the effectiveness of the method proposed in this paper.

2 Related Work

In the research of 3D vision applications, structured light applications, and industrial robot welding trajectory planning, many scholars have done a lot of research work and achieved breakthrough results. Among them, Hao Wang from Jilin University conducted research on three structural light vision assisted welding trajectory recognition and control technologies: laser multi-point positioning, pre weld trajectory fitting, and real-time weld seam tracking. He proposed welding trajectory control models corresponding to the above three models: teaching trajectory correction model, pre weld trajectory fitting model, and real-time weld seam tracking correction model The results show that the laser multi-point positioning and pre weld trajectory fitting mode can efficiently identify the welding trajectory curve before welding, and the welding trajectory basically coincides with the centerline of the weld seam; When welding in real-time tracking mode, the system can correct the deviation of the welding gun in real time. The welding trajectory recognition process and trajectory control model mentioned in the article are sufficient to ensure the stable operation of structured light vision assisted welding [4].

Ruixuan Sun from Hebei Automation Institute has designed a steel grating robot automatic welding system based on 3D vision technology to address the prominent problems of manual completion, poor welding quality consistency, and high labor intensity of steel grating welding processes. By utilizing the 3D vision system, industrial robots, and welding system, high-efficiency and high-quality automated welding of steel grating has been

achieved. The feasibility and scientificity of the method have been verified through practice [5].

Jinyue Liu from Hebei University of Technology proposed a welding trajectory extraction method based on point cloud reconstruction for an unstructured welding scene. After the welding robot changes its work scene, it first detects guiding markers in real time through a depth camera, clarifies the scope and starting point of the work, and reconstructs the scene point cloud. Then, based on point cloud segmentation and boundary extraction algorithms, the weld seam point cloud trajectory is obtained, and a welding robot pose adjustment strategy is proposed. Finally, to address the issue of insufficient point cloud accuracy, laser vision sensors are used to correct the accuracy of welds and extract precise welding trajectories. Through the curve welding scene experiment, it is shown that the robot's motion is smooth, the error in extracting the welding seam trajectory is less than 0.5mm, and the accuracy meets the production requirements [6].

Ruiqi Wang from Beijing Institute of Technology proposed a weld seam tracking method based on line array camera and feature recognition algorithm for near gapless weld seam trajectory under laser welding. Obtain the surface image of the workpiece through a line array camera, and use mean filtering to denoise the image. By analyzing the grayscale values, changes in grayscale values, gradient of grayscale values, and width of the weld seam area, the identification and tracking of seamless welds have been achieved. The welding test results show that the error of the weld seam recognition method based on linear array camera is less than 0 05 mm. By conducting weld seam tracking tests on welds with different gaps, it has been proven that this method is effective for welds with gaps less than 0 The 3mm weld seam has good recognition effect [7].

Yuning Zhang from Dalian University of Technology proposed a robot laser welding trajectory automatic extraction method based on measuring point clouds to achieve automatic welding of freely placed vertical plates beyond the reconstruction from point clouds to CAD models. Simplify the point cloud using uniform sampling method, remove background noise in point cloud measurement using statistical filtering, and perform overall tilt correction on the point cloud. Propose a data scanning strategy to achieve fast segmentation of the top and bottom surfaces of the composite vertical panel. Use distance constraints to improve the RANSAC algorithm and quickly fit the boundary contour of the top surface of the composite vertical panel [8].

In summary, the structure of this article is as follows: Chapter 2 mainly introduces relevant research and summarizes the research results by category. Chapter 3 is an introduction to the construction of visual systems, describing the selection and parameters of each component. Chapter 4 is about weld seam trajectory recognition and trajectory curve fitting. Chapter 5 is the simulation experiment section, which compares the simulation trajectory with the real trajectory to demonstrate the effectiveness of our method. Chapter 6 is the conclusion section, which summarizes the research results of this paper and looks forward to further research.

3 Construction of Visual Welding System

This chapter presents a comprehensive design of a robot welding system based on 3D structured light vision, tailored to actual welding requirements. The system is divided into two components: the visual sensing module and the welding execution module. The main task of the visual sensing part is to obtain weld seam data and process weld seam images, and based on the recognition results, extract weld seam features and plan welding trajectories. The main task of the welding execution part is the execution of welding actions, and the main equipment is industrial robots. In the process of building the welding system, considering the actual working environment of pipe welding, which is affected by factors such as high temperature, dust, and light, this article specifically sets the angle between the structured light plane and the camera axis when designing the visual sensor carrier to enhance the morphological characteristics of the structured light stripes at the weld seam during camera imaging. At the same time, dust-proof and high-temperature resistant equipment is selected. As shown in Fig. 1, the robot welding vision system includes a welding robot, robot control cabinet, welding machine, surface structured light vision sensor, industrial computer, teaching pendant, data processing and data collection equipment, etc [9].

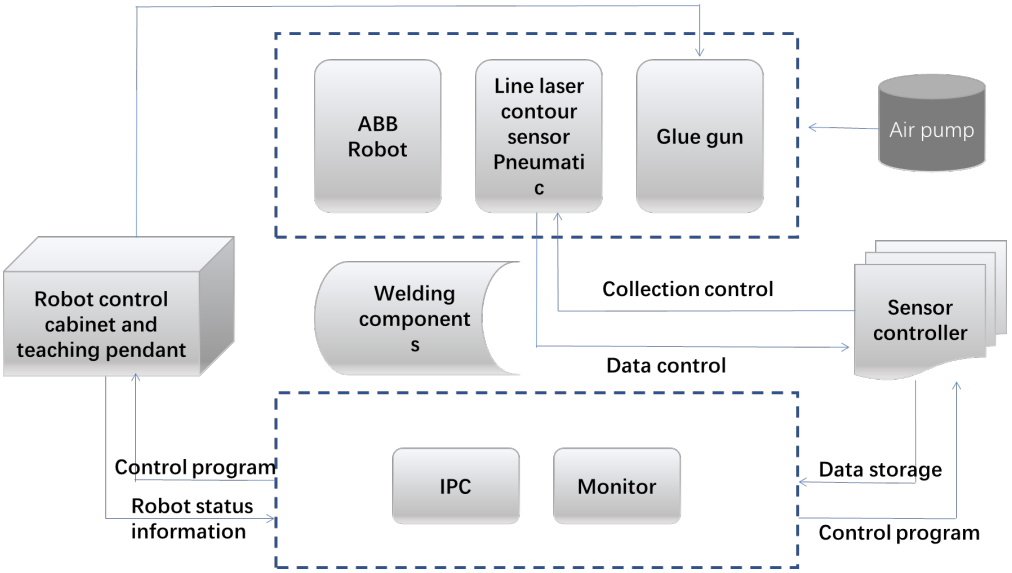

Fig. 1. Robot welding vision system

3.1 Selection of Welding Execution End

The industrial robot adopts ABB IRB-1520ID arc welding robot, and the robot control cabinet model is IRC5. This type of industrial robot has 6 control axes, a maximum load capacity of 4kg, a repeat positioning accuracy of up to 0.05mm, a weight of 170kg, and a reach range of 1.5m. It has many advantages such as high path accuracy, short cycle time, and long pipeline life, and is widely used in the welding field. Due to the common models and products of ABB industrial robots, this article only lists the detailed parameters of the robots. The main technical indicators of the robot are shown in Table 1.

Table 1. Technical parameters related to ABB robots

Parameter	Parameter values
Number of joints	6 joints
Robot body weight	170*kg*
Payload	4*kg*
Maximum reach distance	1.5*m*
Repeatability	0.05*mm*
Absolute positioning accuracy	0.35*mm*

The welding machine selected is the NBM 350U inverter gas shielded welding machine from Shanghai Hugong brand. This type of welding machine uses a photoelectric encoder to provide feedback on the wire feeding speed and length, and combines the high-speed loop control method of an independent chip to control the wire feeding transmission. This welding machine has the characteristics of adjustable arc energy, soft arc, and good welding fusion. It is widely used in the welding of thin and ultra-thin plates such as carbon steel, stainless steel, galvanized plate, and dissimilar metals, especially suitable for bottom welding and all position welding. The welding machine is shown in Fig. 2.

Fig. 2. NBM 350U welding machine

3.2 Visual Sensing Part

The visual sensing part includes a visual sensor and a main control industrial computer. The surface structured light visual sensor is used to obtain three-dimensional data of the welded workpiece, and then the data is transmitted to the industrial computer. The weld seam information is processed in the industrial computer to extract the weld seam information and plan the welding trajectory. The welding trajectory is then transmitted to the industrial robot controller through TCP/IP communication to guide the robot to perform welding. As shown in Fig. 3, the surface structure visual sensor used in this system is the XTOM-MATRIX-3M camera. The camera uses grating projection technology to measure the surface of an object, with blue LED structured light stripes projected onto the surface of the object being measured. The industrial CCD (Charge Couple Device Camera) camera is used to capture the projected structured light pattern, and depth information is calculated based on the demodulation phase. The XTOM-MATRIX-3M camera has a small size and is suitable for assembly at the end of the robot or independent installation and shooting bracket with eye in hand and eye to hand installation methods. It can follow the end to reach more shooting positions and angles, which is very beneficial for use in welding scenes. The detailed parameters of the camera are shown in Table 2.

Table 2. Detailed parameters of camera sensors

Parameter	Parameter values
Camera pixel	3 million
Camera size	380×195×130*mm*
Camera measurement format	200×150*mm*/ 400×300*mm*
Computation speed	<2*s*
Distance between point clouds	0.1*mm*/ 0.2*mm*
Projected light source	Blue light with multiple frequencies
Scanning method	Non contact scanning
Splicing method	Global stitching of landmark points, feature stitching, fully automatic stitching of single or multi axis turntables
Accuracy control	Automatic feedback control, global positioning control
Camera weight	2.4*kg*
Supported systems	Win10 64bits

As the control center of the welding guidance system, industrial computers are an important component of the visual perception system. Industrial computers are equipped with experimental system software and serve as the hardware hub for system data transmission, processing, visualization, and human-computer interaction. The stability and efficiency of industrial computers are the foundation of the overall system. The amount of 3D point cloud data scanned by structured light vision sensors is quite large, and industrial computers need to process a large amount of data in a short period of time, so they must have high-performance central processing units. This article uses Siemens IPC-3000, with the main parameters shown in Table 3.

Table 3. Detailed parameters of industrial computers

Parameter	Parameter values
Motherboard model	Siemens H110 motherboard
CPU model	G4400/I3
CPU heat sink	115X fan
Memory	DDR4 4G
Hard disk	SATA 1T
Power supply	300W industrial power supply
Number of USB ports	6 USB 2.0, 4 USB 3.0
Expansion slot	3 PCI
Interface	Serial port.VGA,DVI,DP
Network card	Gigabit Ethernet port

3.3 Camera Calibration

Machine vision measures and obtains two-dimensional information from target images and surrounding images through visual sensors, and then converts the two-dimensional image information into three-dimensional spatial information through geometric mapping relationships to calculate and understand the three-dimensional world. Before accurate measurement, the camera calibration work needs to be completed first. In this chapter, the Eye to Hand system installation method based on HALCON is calibrated [10]. The calibration diagram is shown in Fig. 3.

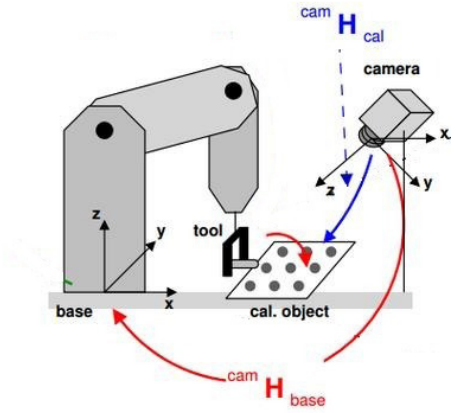

Fig. 3. Eye-to-Hand system diagram

In the Eye-to-Hand system, the camera is installed in a fixed position and does not change position with the movement of the robotic arm. Therefore, the measurement results of the camera on the welded workpiece will not change in angle and distance. The calibration of the hand eye system based on HALCON first involves creating a calibration board according to the size of the experimental object and the description file of the calibration board. As the subsequent calibration of the internal and external parameters of the camera is based on the calibration board, the accuracy of the calibration board will directly affect the calibration accuracy of the camera. This article selects and produces a 30mm x 30mm calibration board based on the installation position of the camera and experimental platform, as well as the size of the images obtained. According to its description file, it mainly consists of black dots with a radius of 0.9375mm arranged 7×7, an outer border of 30mm × 30mm, an inner border of 28.125mm × 28.125mm, and a corner. The centers of the black dots are 3.75mm apart. After the calibration board is made, it is pasted on the support board, placed at different positions in the camera's field of view, and images of the calibration board are taken. Extracting the information of the calibration dots can achieve camera calibration [11].

When calibrating, place the calibration board at different positions on the experimental platform, rotate it in different directions and around different axes, and cover and occupy the entire camera's field of view as much as possible, in order to obtain more accurate internal and external parameters and distortion coefficients. This article conducted three sets of experiments, each obtaining 16 calibration plate images.

In the specific calibration process, the internal parameter matrix Min of the four parameter model is used for calibration, which requires obtaining the camera focal length f, distortion coefficient k, X-axis magnification coefficient S_x, Y-axis magnification coefficient S_y, and optical axis center coordinate point (O_x, O_y). The external parameter matrix of the camera, which requires calculating the rotation angles R_x, R_y, and R_z of the camera coordinate system around the world coordinate system, is represented as follows:

$$R_x = \begin{bmatrix} 1 & 0 & 0 \\ 0 & \cos\alpha & \sin\alpha \\ 0 & \sin\alpha & \cos\alpha \end{bmatrix} \tag{1}$$

$$R_y = \begin{bmatrix} \cos\beta & 0 & \sin\beta \\ 0 & 1 & 0 \\ -\sin\beta & 0 & \cos\beta \end{bmatrix} \tag{2}$$

$$R_z = \begin{bmatrix} \cos\gamma & \sin\gamma & 0 \\ \sin\gamma & \cos\gamma & 0 \\ 0 & 0 & 1 \end{bmatrix} \tag{3}$$

In the equation, α, β, γ is the Euler angle of rotation of the end coordinate system relative to the base coordinate system. Based on HALCON calibration, the specific steps are shown in Fig. 4.

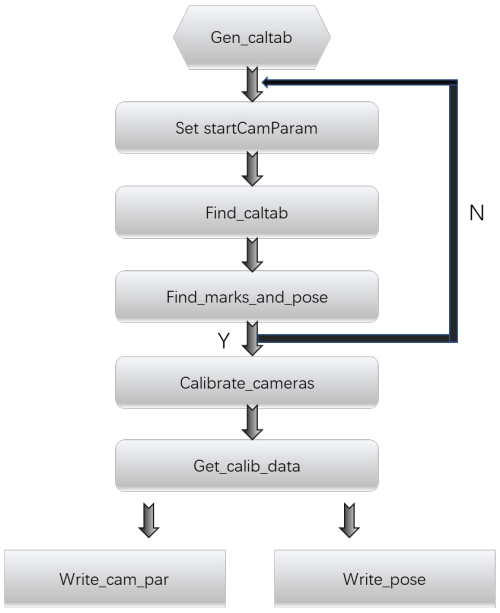

Fig. 4. Detailed steps based on HALCON calibration

After the above algorithm, for the Eye-to-Hand system, the installation position of the camera remains fixed, so the internal parameters of the camera obtained from calibration remain unchanged, while the external parameters of the camera may change with the position of the calibration plate. However, as long as we know the po-

sition of the camera relative to a fixed point, in the subsequent template matching recognition, we can calculate the actual deviation in the world coordinate system based on the position difference between the real-time image and the template image in the image coordinate system. At the same time, when calibrating the camera, due to the large difference between the calibration result and the focal length of the camera lens, it is because the focal length of the lens can be adjusted. In the experiment, the focal length was adjusted based on the clarity of the image, rather than fixed focal length. On the basis of the internal and external parameters of the camera calibrated above, images were taken and several points were selected on the image. The pixel coordinates of each point in the image were converted into world coordinates, and the converted world coordinate values were compared with the actual coordinate values to verify the accuracy and precision of the camera calibration results. At the same time, input the world coordinate values on the human-computer interaction platform, convert them into image coordinate values based on the calibration results, and mark the positions and coordinate values of their points in the image.

This chapter has completed the selection of the visual system, calibrated the camera, and built the visual part. The next chapter will implement the recognition and extraction of weld seam features based on this chapter.

4 Weld Seam Feature Extraction and Path Planning

The welding object studied in this article is metal pipes. The welding of pipes is generally circular welds and intersecting line welds. The structure of circular welds is simple, the welding process is single, and the intersecting line welds belong to spatial structures with relatively complex trajectories. Therefore, this article focuses on the intersecting line welds of pipe welding components. The intersecting line of pipe fittings is a spatial curve formed by the intersection of the neutral axis surfaces of two circular pipe walls, which is a typical irregular curve. The intersecting line welds are spatial curves composed of welding points during the welding process. The shape of the intersecting line welds is similar to that of a saddle, so the intersecting line welds are also called saddle shaped welds. The top view is a standard circular curve, but there is a height difference in the vertical direction, commonly referred to as a saddle shaped drop. On the basis of extracting typical intersecting line welds, this section completes the planning of industrial robot trajectories.

The mathematical model of intersecting weld seam is the core prerequisite for determining the design of robot structure scheme and realizing the motion control of welding robot. When using a welding robot to weld intersecting line welds, a mathematical description of the weld seam must be provided as the target condition for robot trajectory planning. In actual production, the intersecting weld seam is generally divided into four types: orthogonal, oblique, orthogonal offset, and oblique offset, based on the deflection angle and distance between the axes formed by the intersection of two pipelines. This article takes orthogonal intersecting lines as the research object. In order to maintain generality, let two circular pipes intersect orthogonally with any diameter, and let the diameters of the two pipes be r_1 and r_2, respectively. Orthogonal means that the axes of two circular tubes are perpendicular to each other. The angle of rotation of the horizontal circular tube is θ, which is the angle between the OA' and x axes, as shown in Fig. 5.

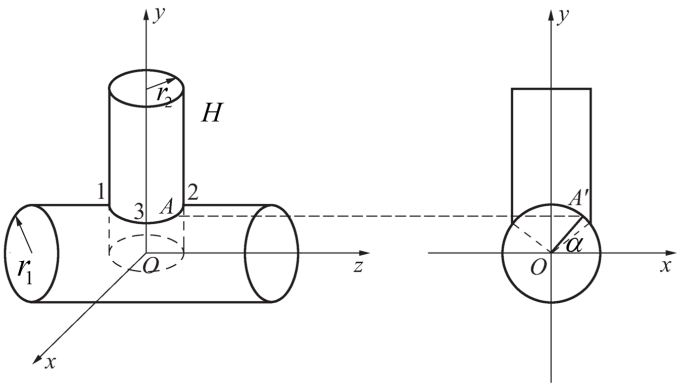

Fig. 5. Schematic diagram of orthogonal intersecting lines

In coordinate system *Oxy*, the equations for a horizontal circular tube and a vertical circular tube are expressed as follows:

$$\begin{cases} x^2 + y^2 = r_1^2 & z \in [-H, H] \\ x^2 + z^2 = r_2^2 & y \in [0, h] \end{cases} \tag{4}$$

Substitute the two into the parameter equation of the intersecting line:

$$\begin{cases} x = r_1 \cdot \cos\alpha \\ y = r_1 \cdot \sin\alpha \\ z = H \end{cases} \tag{5}$$

Further use two pipe radii to represent the value of *H*:

$$z = \sqrt{r_2^2 - (r_1 \cos\alpha)^2} \tag{6}$$

$$\alpha \in \left[\arccos\frac{r_2}{r_1}, \pi - \arccos\frac{r_2}{r_1} \right] \tag{7}$$

The range of variation for α is between the two dashed lines, and for $r_1 = r_2$, the projection of the intersecting line in the *Oxy* plane becomes a semicircle with a range of variation of [0º, 180º]. Since the establishment of this equation is based on the arc length moved by any point *P* on the intersecting line during the rotational motion in time *t*, it should match the distance advanced by the robot's end welding gun in time *t*. Due to the fact that the trajectory of *P* is a curve with non-linear changes, the theory of calculus can be used to calculate the arc length generated at any time at point *P*. However, in the actual welding process, the mechanical structure cannot achieve accurate fitting. Therefore, this article uses the actual distance *l* moved by point *P* in *t* time to approximate the arc length *s* in *t* time.

The typical intersecting line welds are shown in Fig. 6.

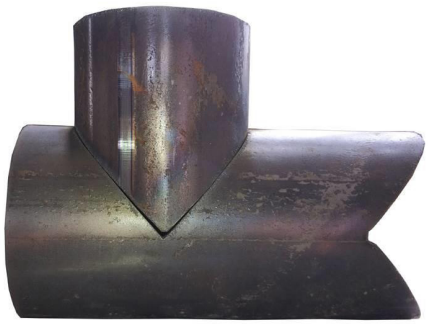

Fig. 6. Schematic diagram of pipe welding structure

4.1 Inspection of Pipe Fittings Welds

The surface of the pipe is relatively smooth, resulting in a high light reflectivity on the metal surface. In practical visual recognition applications, adjusting the light intensity often requires the use of additional lighting equipment. Although lighting equipment can effectively adjust the intensity of light, it can lead to an increase in the

cost of visual sensing systems. In order to achieve equivalent adjustment of lighting intensity, methods such as adjusting the exposure time of image capture and controlling the duration of diffuse reflection light captured by visual sensors can be used.

1) Image preprocessing, the typical feature of the weld seam in the image is the sharp change in grayscale values at the weld seam, which is called the edge or contour feature of the image in computer vision [12]. During image recognition, the region of interest (ROI) of the image is set, and the result is shown in Fig. 7.

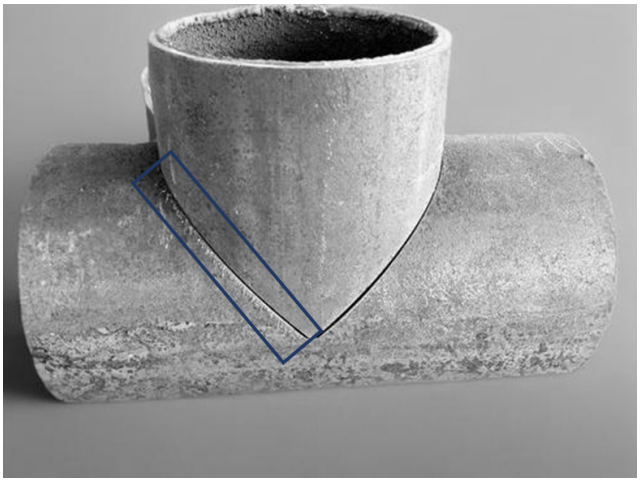

Fig. 7. ROI setting for the intersection line of pipe fittings

2) Edge feature extraction. The most commonly used edge detection method for weld seam detection in images is the differential operator method, which detects each pixel in the area based on the grayscale value changes of the image, and uses the first-order or second-order directional derivatives close to the edge to detect the edge. This article uses an improved Candy algorithm [13] to extract features from the edges of pipe welds. Firstly, convert the captured image into a grayscale image and define the grayscale image as $G(x_i, y_i)$. Gaussian filtering is applied to grayscale images to reduce noise in the image [14]. Then, calculate the pixel gradient based on the different directions of the pixel plane coordinate axis:

$$\begin{cases} Grad_x = Sob_x * G \\ Grad_y = Sob_y * G \end{cases} \tag{8}$$

In the formula, Sob_x and Sob_y are the *Sobel* operators of the pixel points on the *X*-axis and *Y*-axis of the pixel plane coordinate system, respectively. Further calculation yields the gradient values of each pixel point.

$$grad_{xy}(x_i, y_i) = \sqrt{grad_x^2(x_i, y_i) + grad_y^2(x_i, y_i)} \tag{9}$$

Then obtain the gradient direction of the pixel points:

$$d_{gra} = \arctan\left(grad_x(x_i, y_i) \Big/ grad_y(x_i, y_i) \right) \tag{10}$$

The schematic diagram of the algorithm principle is shown in Fig. 8.

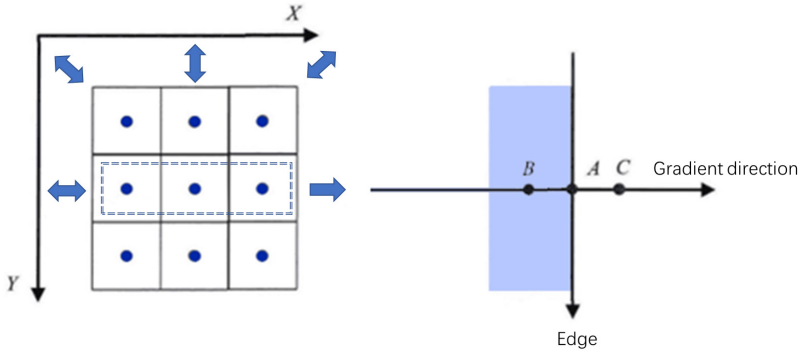

Fig. 8. Schematic diagram of algorithm principle

In order to obtain more accurate edge positions, the categories of gradient directions were reduced from the 4 categories of Canny edges to 2 categories, namely horizontal and vertical directions. When condition $g_x(x_i, y_i) \geq g_y(x_i, y_i)$ is met, the gradient direction is horizontal, otherwise it is vertical. The non maximum suppression method is also used to screen edge pixels. When the gradient direction is reduced to two categories, the edge points in the image can be reduced, making the obtained edge features more accurate. The comparison of the improved algorithm's performance is shown in Fig. 9.

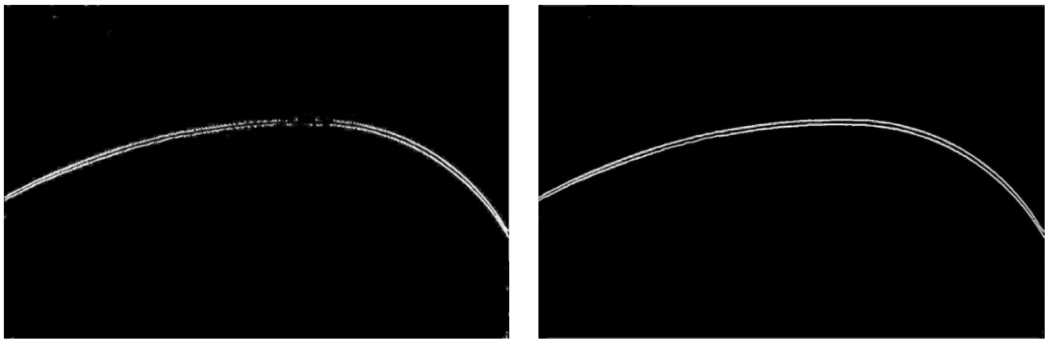

Fig. 9. Edge detection results

3) Noise reduction processing, there is still some noise in the ROI area. Connect edge pixels through a certain pattern to form an edge chain, and the gradient direction difference of edge pixels connects them. Assuming that the gradient direction of edge pixel A is d_{graA} and the gradient direction of edge pixel B adjacent to pixel A is d_{graB} [15], the condition for these two edge pixels to be connected together is:

$$\begin{cases} |p_{xa} - p_{xb}| < \Delta_a \\ |p_{ya} - p_{yb}| < \Delta_b \\ |d_{graA} - d_{graB}| < \Delta d \end{cases} \tag{11}$$

In the formula, (p_{xa}, p_{ya}) and (p_{xb}, p_{yb}) are the coordinates of pixel A and pixel B in the image, respectively, and Δ_a and Δ_b are the positional deviation thresholds of pixel A and pixel B in the horizontal and vertical coordinates of the image, respectively; Δd is the threshold between edge pixel point A and edge pixel point B in the gradient direction. Edge pixels are connected to each other to form an edge chain. The length of the edge chain is defined

as the number of edge pixels in the edge chain, which can be reduced or filtered according to the length of the edge chain. Setting length and gradient thresholds can effectively remove noise points in feature recognition. Set the gradient threshold range to [10, 20], $\Delta_a = 2$, $\Delta_b = 2$, $\Delta d = 60^{\circ}$. The final weld seam feature recognition result is shown in Fig. 10.

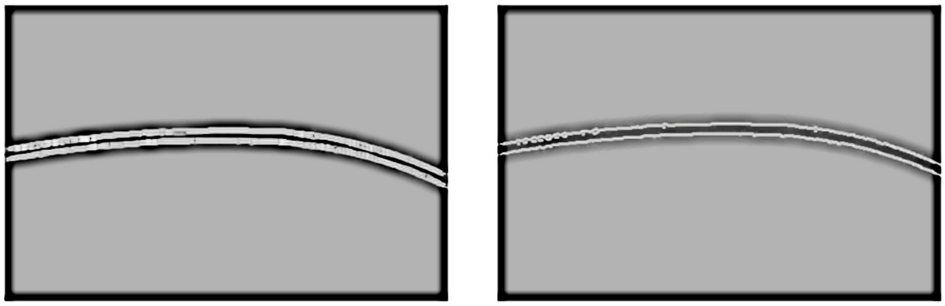

Fig. 10. Edge detection results

4.2 Fitting of Weld Trajectory

This section mainly achieves complete weld seam detection and extracts welding trajectory point clouds through the image weld seam detection results and their corresponding depth maps. In addition, due to the large number of points extracted from the welding trajectory point cloud and the different distances between points in the welding trajectory point cloud, curve fitting is performed on the welding trajectory point cloud after obtaining the complete welding trajectory point cloud. Set an ROI region in the depth map, starting from the center of the edge chain representing the weld seam in the image, and spreading towards both ends of the edge chain; Establish a straight line with the gradient direction of each edge pixel point as the direction vector and passing through the edge pixel point. The straight line is centered on the edge pixel point and has a length of segment A in the pixel plane; Calculate the pixel coordinates covered by the line segment and obtain the corresponding depth information for each pixel based on the depth map. Extract the point cloud trajectory of the weld seam using the welding form of the workpiece shown in Fig. 6. Assuming B, the depth curve trajectory point cloud of the weld seam is shown in Fig. 11.

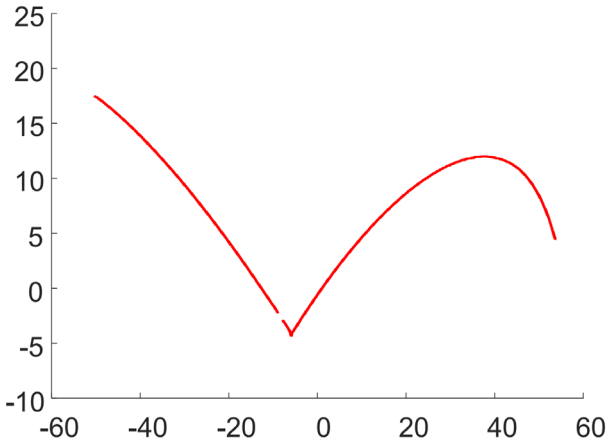

Fig. 11. Intersection line trajectory

In order to better represent the welding trajectory, it is necessary to perform curve fitting interpolation on the welding trajectory point cloud. In this paper, B-spline curves are used for fitting, and the trajectory point cloud is defined as $Pcloud = \{Pcloud_1, \ldots, Pcloud_N\}$ [16], where N is the number of welding trajectory point clouds. The fitting expression of B-spline curve is as follows:

$$B(t) = \sum_{n=1}^{N} B_{n,d}(t) \tag{12}$$

In the equation, $d = 4$, assuming the number of control points is known, finding the position of the control points in the known welding trajectory point cloud can be transformed into solving the minimization objective equation, where the objective equation can be written as:

$$f(t) = \sum_{n=1}^{N} d^2\left(B(t), Pcloud_n\right) \tag{13}$$

Among them, $d(B(t), Pcloud_n) = \min_t \left\| B(t) - Pcloud_n \right\|$ represents the minimum Euclidean distance from point $Pcloud_N$ to the B-spline curve. The minimization of the objective equation can be achieved by taking the first derivative of each control point, which is expressed as follows:

$$\frac{df(t)}{dB(t)} = \sum_{n=1}^{N} B_{n,d}(t_n) - \sum_{j=1}^{N} B_{n,d}(t_j) Pcloud_j \tag{14}$$

If the first derivative of the control point is equal to 0 and the number of control points on the curve is set to 10, the fitted trajectory curve is shown in Fig. 12.

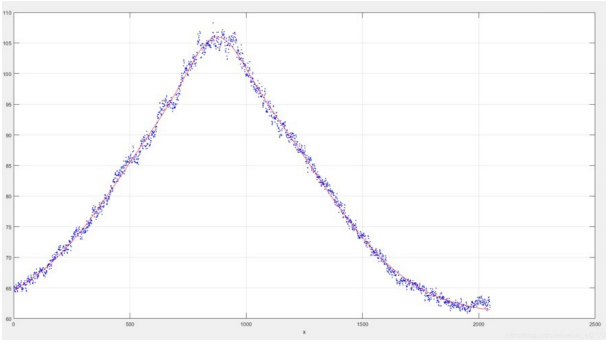

Fig. 12. Trajectory fitting results

4.3 Welding Trajectory Planning

After the fitting of the welding trajectory point cloud is completed, trajectory planning is carried out, that is, the pose planning of the welding gun at the end of the robot is completed. When the three-dimensional model of the workpiece is known, the corresponding welding gun pose can be obtained by comparing the real welding trajectory with the theoretical welding trajectory. But when the 3D model of the workpiece is unknown, it is necessary to establish a welding point coordinate system based on local point cloud information to achieve welding trajectory planning. To maintain generality, it is assumed that the three-dimensional model of the workpiece is unknown. When using a 3D model of the workpiece for welding trajectory planning in an offline environment, the Z_s-axis is generally determined by the normal vectors of the cutting planes on both sides of the weld seam. In the point cloud, it is necessary to approximate the local point cloud of the current welding point as a plane and

calculate its normal vector. However, the normal vector of the local point cloud of the welding point is usually difficult to solve, and the accuracy of the normal vector is far inferior to that obtained from the 3D model. The overall process of trajectory planning is shown in Fig. 13.

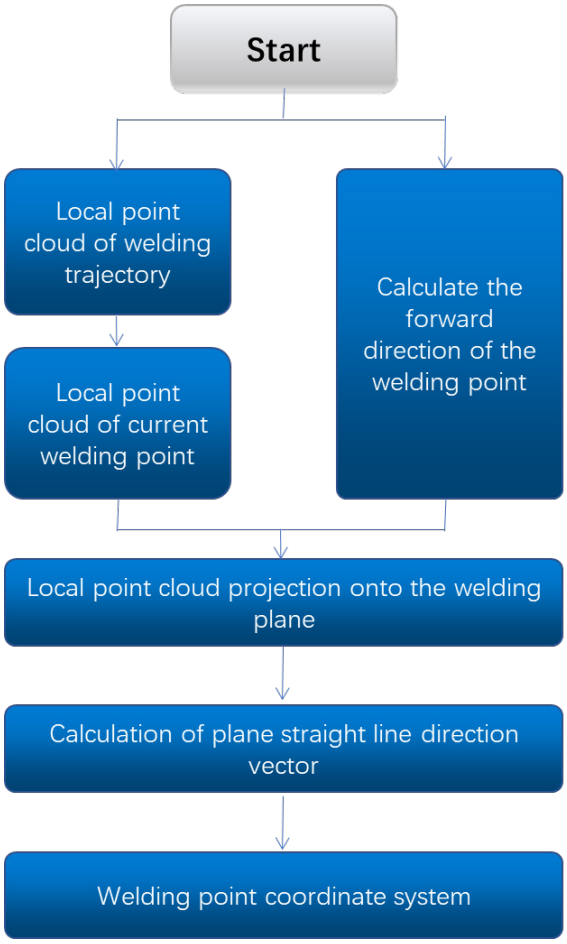

Fig. 13. Trajectory planning flowchart

In order to prevent physical interference between the welding gun installed on the robot and the weld groove wall, it is necessary to plan the posture of the welding gun. For A-type welds, the posture of the welding gun is mainly affected by the contour feature points of the weld. The weld trajectory of the travel generally does not include the dynamic changes of the welding gun, and the angle of the welding gun should change in real time with the welding process. This paper proposes a weld trajectory optimization algorithm based on pose interpolation. Firstly, the weld trajectory data is preprocessed to obtain the weld trajectory downsampling data. To reduce sampling errors, the sampled weld trajectory is fitted with a cubic B-spline algorithm. Then use the fitted data points as shape points, and interpolate the position and orientation of the weld seam trajectory using the cubic B-spline algorithm and Squad algorithm [17], respectively. This algorithm optimizes both the position and posture of the weld seam trajectory, ensuring smooth pose transformation and improving the stability and accuracy of the robot's welding motion. The algorithm flowchart is shown in Fig. 14.

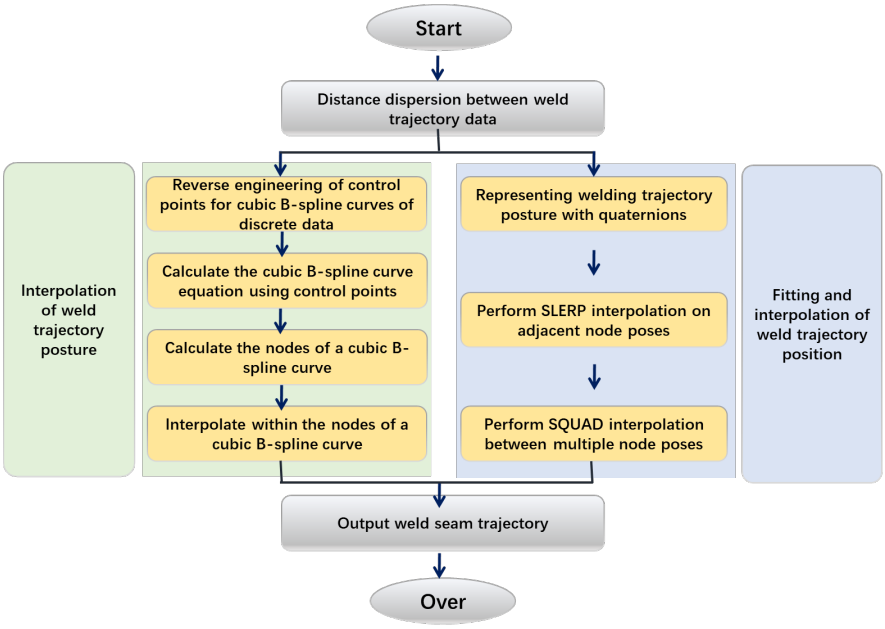

Fig. 14. Squad algorithm process

After the above process, the description of the welding trajectory planning method has been completed.

5 Experiment and Results Analysis of Weld Seam Trajectory Planning

This section mainly verifies the error between the planned welding trajectory and the actual trajectory through simulation experiments, and analyzes the error results. Firstly, the cubic B-spline interpolation algorithm is used to interpolate 10 position and attitude data between every two welding points on the welding trajectory, and correspond them one by one. The obtained trajectory curve is shown in Fig. 15.

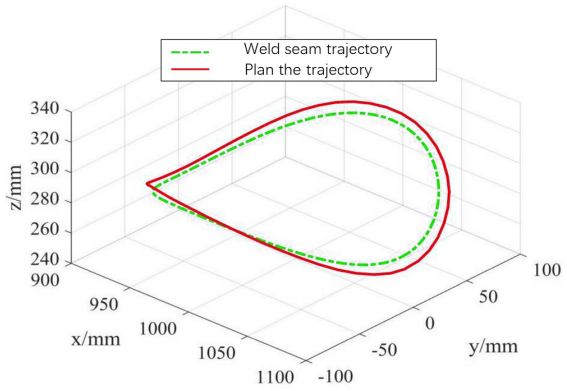

Fig. 15. Weld trajectory curve

5.1 Analysis of the Effectiveness of Weld Trajectory

In order to study the optimization effect of welding trajectory, the smoothness of weld trajectory is analyzed. When the position of the welding trajectory is smooth, the change in the tangent direction of the welding point should also be a continuous smooth change; When the posture of the welding trajectory changes smoothly, the changes in each coordinate axis should also be continuous and smooth. As stated in section 4.1, the tangent direction of the welding point can be approximated as the Y-axis direction of the welding point coordinate system. Therefore, it is only necessary to statistically analyze the angle changes of each coordinate axis of adjacent welding feature points in the welding trajectory to verify the smoothness of the welding trajectory. For the convenience of research, this article analyzes the welding trajectory of intersecting line welds as the research object. Using the pre optimized weld seam feature points as the search object, calculate the weld seam trajectory composed of the optimized weld seam feature points and the nearest point to the pre optimized weld seam feature points as the comparison object. Calculate the attitude changes of adjacent weld seam feature points in the intersecting weld seam before and after optimization separately, and record them. The posture change of the optimized intersecting line weld seam is shown in Fig. 16. It can be seen from the figure that after optimizing the weld seam trajectory, the posture change of the weld seam trajectory is uniform, and the maximum angle change does not exceed 0.2 °, which meets the welding requirements.

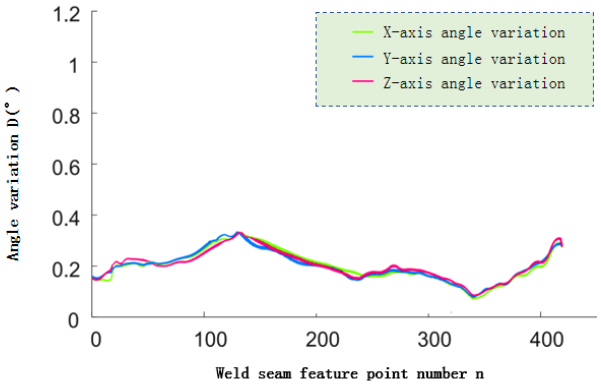

Fig. 16. Optimized welding trajectory angle change

5.2 Analysis of Welding Trajectory Error

Calculate the maximum error and root mean square error of each axis component of the welding trajectory in the spatial coordinate system separately. The formula for calculating the root mean square error of welding trajectory is as follows:

$$E_{error} = \sqrt{\frac{1}{N}\sum_{i=1}^{N}\left|p_i - q_i\right|^2} \tag{15}$$

$$\begin{cases} \lambda_{error} = \sqrt{\dfrac{1}{N}\sum_{I=1}^{N}\left(\arccos\left(Z_i\right)\right)^2} \\ \lambda_{\max} = \max\left\{\arccos\left(Z_i\right)\right\} \end{cases} \tag{16}$$

After calculation, the error values are shown in Table 4. The maximum position error of 1.56mm is the component on the Z-axis, and the maximum attitude error is 0.195rad, with the maximum errors located near the endpoints of the welding trajectory. But the root mean square error is not significant, meeting the precision requirements for robot welding.

Table 4. Weld seam error analysis

Weld seam name	Root mean square error	Standard deviation	Average deviation
Intersection line weld seam	0.1789mm	0.1367mm	0.2487mm

This section completed the experimental simulation of trajectory planning for orthogonal intersecting line welds, and evaluated the simulation results by calculating the maximum error and root mean square error of the trajectory. The final results proved that the trajectory planning method provided in this paper can meet the actual production needs and achieve the expected accuracy.

6 Conclusion

This article focuses on the main problems faced by automated welding of pipes and the welding of intersecting line welds. Using a six degree of freedom welding robot, a feature extraction and trajectory planning method is designed for intersecting line welds. The focus was on how the visual system can quickly and accurately extract weld seam information, and through joint motion optimization of the welding robot, automated welding of intersecting line welds was achieved. The rationality of the planning was verified through experiments, and the following results were summarized:

1) Studied the entire visual system. Using a high-precision black and white point calibration board significantly reduces the calibration results of the camera's internal and external parameters. Establish a calibration method for structured light planes and obtain the calibration light plane coefficients.

2) The centerline extraction of the weld seam image trajectory has been completed. Using linear filtering to remove image noise from the weld seam images obtained by the camera, a clear and complete weld seam contour is obtained. And through the improved Canny edge detection algorithm, better than general algorithms for weld seam edges were obtained. Further curve fitting was performed to extract the centerline and obtain the coordinate information of the weld seam, providing parameters for subsequent robot trajectory planning.

3) Studied trajectory planning algorithms. By avoiding singular robot configurations and ensuring smooth motion, genetic algorithm is used to optimize the joint motion of the robot, which improves the convergence speed of global optimal solution search. Through simulation analysis, the adjusted joint motion trajectory is smoother, verifying the efficiency of the trajectory planning method.

This article also has research shortcomings, and further research directions are:

1) The experiments in the research process of this article were all completed in the laboratory, and there is a lack of complete welding experiments. Further research and analysis of the welding environment will be conducted to supplement the welding experiments. And verify the differences in the effectiveness of the algorithm in processing different working conditions in actual welding environments.

2) Research can be conducted on other types of welds to expand the diversity of weld treatment types; Improve the optimization of the software part to make the processing faster and more efficient.

3) The intersection line selected in this article is a relatively simple intersection line category among all intersection line categories. At the same time, the most complex trajectory in the intersection line category is the offset oblique intersection line. However, in order to establish a more general intersection line equation, in the direction of intersection line trajectory recognition, it is more important to establish intersection line equations for all categories, generate fitting curves for all intersection line categories, and complete the recognition and classification of intersection line trajectories for all categories.

References

[1] H.-L. Zeng, M.-X. Yang, H.-J. Gui, J.-Z. Qi, Review of welding and testing technology of long distance pipeline, Petroleum Engineering Construction 47(S1)(2021) 7-12.
[2] X.-L. Xu, Z. Fang, H. Zhang, Y. Luo, L. Zhang, J.-F. Wu, G.-T. Ma, A.-D. Zhang, S.-Y. Zhang, Development and Application of Automatic Welding System for Steel Sater Supply Sipe in Urban Underground Comprehensive Pipe Gallery, Electric Welding Machine 52(8)(2022) 57-64.
[3] B. Peng, Y. Cao, X.-T. Deng, Z.-Q. Chen, Y. Li, S.-X. Xu, J.-M. Zhang, Vision Based Inspection Method for Large Area Tube-plate Welds and Design of Inspection System, Dongfang Electric Review 37(3)(2023) 62-66.
[4] H. Wang, X.-H. Zhao, L.-Z. Xu, H. Jiang, Y. Liu, Research on trajectory recognition and control technology of structured light vision-assisted welding, Transactions of the China Welding Institution 44(6)(2023) 50-57+132.
[5] R.-X. Sun, H.-Q. Hao, L. Xiao, C. Chen, Design and implementation of robot automatic welding system of steel grating based on 3D vision technology, Journal of the Hebei Academy of Sciences 41(1)(2024) 28-32.
[6] J.-Y. Liu, W.-X. Li, X.-H. Jia, C.-Y. Feng, Operation trajectory extraction method of mobile welding robot based on point cloud reconstruction, Computer Integrated Manufacturing Systems 30(7)(2024) 2381-2388.
[7] R.-Q. Wang, Y. Zhao, S.-K. Wu, H.-T. Lu, Multifeature Recognition Methods of Laser Welding Based on Line Array Camera, Laser & Optoelectronics Progress 60(1)(2023) 239-246.
[8] Y.-N. Zhang, J.-N. Guan, L.-N. Zhu, T. Pan, J.-T. Xu, Automatic Extraction Method of Welding Trajectory from Point Cloud for Robotic Laser Welding, Machine Tool & Hydraulics 51(11)(2023) 7-12.
[9] S. Liu, L. Zhang, L.-H. Gao, X. Li, D.-Z. Zhao, Automatic welding system for large pipe based on machine vision, Journal of the Hebei Academy of Sciences 40(1)(2023) 26-29.
[10] Q. Cheng, H. Huang, J.-J. Xu, J.-H. Li, Y. Li, T. Zhang, An efficient robot hand-eye calibration method based on binocular vision and Halcon, Modern Electronics Technique 46(13)(2023) 35-42.
[11] Q. Sun, Z.-Z. Luo, The Research of Plane Part Recognition Based on the Eye-to-hand Robot System, Journal of Hangzhou Dianzi University 30(1)(2010) 46-49.
[12] Q. Yang, S.-S. Fan, Visual navigation method for electric power inspection robot based on image preprocessing and semantic segmentation, Journal of Electric Power Science and Technology 38(6)(2023) 248-258.
[13] C.-X. Xi, S.-J. Guan, Air compressor crankshaft profile extraction based on improved Canny operator, Journal of Xiangtan University (Natural Science Edition) 45(6)(2023) 110-115.
[14] K. Wen, J. Ji, X. Xue, R.-J. He, Image denoising method based on edge feature fusion network, Microelectronics & Computer 40(6)(2023) 25-32.
[15] F.-Y. Wang, F. Zhang, J.-Y. Du, H.-L. Lei, X.-F. Qi, Adversarial Examples Detection Method Based on Image Denoising and Compression, Computer Engineering 49(10)(2023) 230-238.
[16] X.-X. Duan, D. Miao, Y.-M. Wang, Y.-L. Sun, A laser detection method for belt conveyor coal flow based on B-sample curve fitting, Journal of Tianjin University of Technology and Education 34(2)(2024) 56-61.
[17] C.-Q. Qian, Y. Ou, H.-T. Feng, J.-P. Huang, Quaternion interpolation algorithm evaluation method based on unit spherical trajectory, Machine Design and Manufacturing Engineering 50(3)(2021) 28-33.